Egypt. J. Chem. **Vol. 66**, No. 9. pp. 271 - 291 (2023)

Egyptian Journal of Chemistry

http://ejchem.journals.ekb.eg/

Raman and Infrared Spectral Analysis, Normal Coordinate Analysis, DFT calculations of Novel Schiff Base Containing di-imine moieties

Ahmed. Nasser[a, b*], M. A. Migahed[b], N. M. EL Basiony [b, c], H. M. Abd-El-Bary[d], Tarek A. Mohamed[*d]

[a]*The Higher Institute of Engineering, New Elmarg, El-Qalyubia, Egypt.*

[b]*Egyptian Petroleum Research Institute, Nasr City 11727, Cairo, Egypt.*

[c]*School of Chemical Engineering, Sungkyunkwan University, Suwon 16419, Republic of Korea.*

[d]*Department of Chemistry, Faculty of Science (Men's Campus), Al-Azhar University, Cairo, Egypt.*

Abstract

The Raman (3500−100 cm^{-1}) and mid-infrared (4000−400 cm^{-1}) spectra in addition to the ^1H NMR chemical shifts (δ, ppm) of ((*N*[1]*Z*, *N*[4]*E*)-*N*[1], *N*[4]-bis (4 (dimethylamino) benzylidene) butane 1,4-diamine) Schiff base (Molecular formula, $C_{22}H_{30}N_4$) has been recorded. Moreover, we have carried out full geometry optimization followed by frequency calculations using the DFT-B3LYP method employing 6-31+G(d) basis set to include the polarization and diffusion functions. The Raman activities and infra intensities favour a slightly distorted symmetric molecule with an inversion center. Aided by the calculated wavenumbers assembled with Raman and infrared spectral observations, we have provided complete/reliable vibrational assignments for all fundamentals with the exception of those anticipated below 100 and 400 cm^{-1}, respectively, this is true regardless of whether or not any fundamentals were found either overlapped or coincident. Analyses of normal coordinates provide support for the prevailing spectral interpretations, that were based on the computed atomic displacements in x, y and z Cartesian coordinate (ADCC) from B3LYP/6-31+G(d). All results are reported herein and compared with similar molecules whenever appropriate.

*Keywords:*Schiff base; Infrared; Raman; Vibrational Assignment and DFT.

1. Introduction

Schiff bases are classified as a subclass of imines (R_1>C=N– R′), R′≠H, known as azomethines and could be considered as nitrogen analog of an aldehyde or ketone [1]. Otherwise, they are categorized as uni-, di-, tri-, and tetra-dentate ligands depending on the number of donor atoms in which the nature of the primary amine/diamine and the type of aldehyde/ketone determine the donor nature [2,3]. Schiff bases/imines are crucial synthetic intermediates [4], they are widely used in design of chemosensors/probes, detection of various toxic analytes, agriculture, imaging of various analytes in biological systems and molecular recognition [5-7]. There are numerous uses for Schiff base complexes, including pharmaceutical [8], medical/antimicrobial fields (drug delivery, cancer, diagnosis, tissue regeneration, wound healing, tissue adhesives) [9-11], bioinorganic chemistry, water treatment, catalysis, material science, supramolecular chemistry, separation and/or encapsulation processes as well as in the development of substances with unique structural features [12, 13]. Moreover, Schiff bases have been proven to be efficient at preventing corrosion [14-16]. Therefore, the organic/inorganic framework of Schiff bases and their applications are brought to the attention of computational chemists

*Corresponding author e-mail: **Tarek A. Mohamed**: tarek_ama@azhar.edu.eg; **Ahmed.Nasser:**Ahmednasser1992@outlook.com
EJCHEM use only: Received date 2022-11-02; revised date 2022-12-19; accepted 2022-12-22
DOI: 10.21608/EJCHEM.2022.172441.7143

through DFT simulations, and molecular modelling/docking approaches/procedures [8, 17-21] in addition to vibrational analysis [8, 22-27]. The ((*N*[1]*Z*, *N*[4]*E*)-*N*[1], *N*[4]-bis (4 (dimethylamino) benzylidene) butane 1,4-diamine) Schiff base is a promising corrosion inhibitor owing to the presence of two benzylidene rings and four nitrogen atoms. According to the literature survey and to the best of our knowledge neither vibrational nor computations were reported elsewhere for Schiff-B; MF $C_{22}H_{30}N_4$. Therefore, we have initiated the current vibrational (Raman and infrared) in addition to ^{1}H NMR spectral investigations. Further computations, using LCAO-MO-SCF quantum mechanical (QM) optimization followed by wavenumbers predictions were also carried out using DFT-B3LYP/6-31+G(d) basis set [28]. Aided by normal coordinate analysis using the produced atomic displacements of Cartesian coordinate (ADCC) in x, y and z directions, we can provide reliable and confident vibrational interpretations of the observed Raman and infrared bands. The results will be compared with similar molecules whenever appropriate.

2. Experimental

2.1. Chemicals

High purity grade used chemicals in this study were used purchased from alpha chemical company and have been used without further purification from various companies with as follow; 4-(Dimethyl amino) benzaldehyde, 1,4-Diaminobutane, Ethanol.

2.2. Synthesis of the Schiff Base

The Schiff-B was prepared using round flask fitted with water-cooled condenser. The 4-(Dimethylamino) benzaldehyde and 1,4-Diaminobutane (2:1 molar ratio in 25 mL of EtOH) were refluxed in a heating mantel with three droplets of HCl for 7h at 80°C with continuous stirring to yield ((*N*[1]*Z*, *N*[4]*E*)-*N*[1], *N*[4]-*bis* (4 (dimethyl amino) benzylidene) butane 1,4-diamine), as shown in Scheme 1[29]. Adding HCl were kept to a minimum to avoid the protonation of imine nitrogen atom(s). After cooling, the product is filtered out and recrystallized from absolute ethanol, 82% percentage yield was obtained and m.p of 130 °C was reported using Melting point apparatus (Stuart Scientific Co. Ltd).

2.3 Structural Characterization of Schiff-B

Structural characterizations of the synthesized "((*N*[1]*Z*, *N*[4]*E*)-*N*[1], *N*[4]-*bis* (4 (dimethyl amino) benzylidene) butane 1,4-diamine), Molecular formula: $C_{22}H_{30}N_4$" have been emphasized by elemental analysis, infrared-, Raman- and NMR-spectroscopic measurements, Figures 1A, 1B and Fig.2, respectively. CHNanalysis were obtained using a Vario Elementar Analyzer (Hanau, Germany) [30], the revealed (Calc/found) percentages were as follow; C: (75.39/75.30), H: (8.63/8.21) and N: (15.98/15.88). ^{1}HNMR, DMSO (Fig. 2): δ 2.9 (s, 12 H, 4 CH_3), 1.59 (m, 4H, 2CH_2), 3.48 (t, 4H, 2CH_2), 6.7 (d, 2H, J = 8.00 Hz, Ar-H), 7.5 (d, 2H, J = 7.33 Hz, Ar-H), 8.76 (s, 2H, CH enaminic). The vibrational spectra of the reactant's molecules have been already published; IR and Raman spectra of 4-dimethylaminobenzaldehyde [31] in addition to the IR spectrum of butane-1,4-diamine [32]. The absence of the vibrational signatures of both the aldehyde and amino moieties confirms the formation of Schiff-B. The characteristic group frequencies of the carbonyl stretch were observed earlier [31] at 1666 (ms; R) is vanished herein. Whereas the sharp Raman bands at 1588 (vs) and 1552 (w) [31] were split herein at 1638 (vs) and 1607 (vs), considering C=N and C=C stretching modes. In addition to that, the IR extensive broadening from 2200-3500 cm^{-1} owing to primary amine(s) hydrogen bonding (HB) interactions [31] were cleared-out in the IR spectrum of the investigated Schiff-B (**Fig. 1A**). Nevertheless, the observed Raman band above 3100 cm^{-1} owing to intermolecular HB NH_2 for 1,4-diaminobutane [32] is absent in the Raman spectrum of Schiff-B (**Fig. 1B**). We will discuss in detail IR and Raman vibrational interpretations of our Schiff-B based on B3LYP/6-31+G(d) estimated frequencies, assisted by normal coordinate analysis based on atomic displacements in Cartesian coordinate (ADCC).

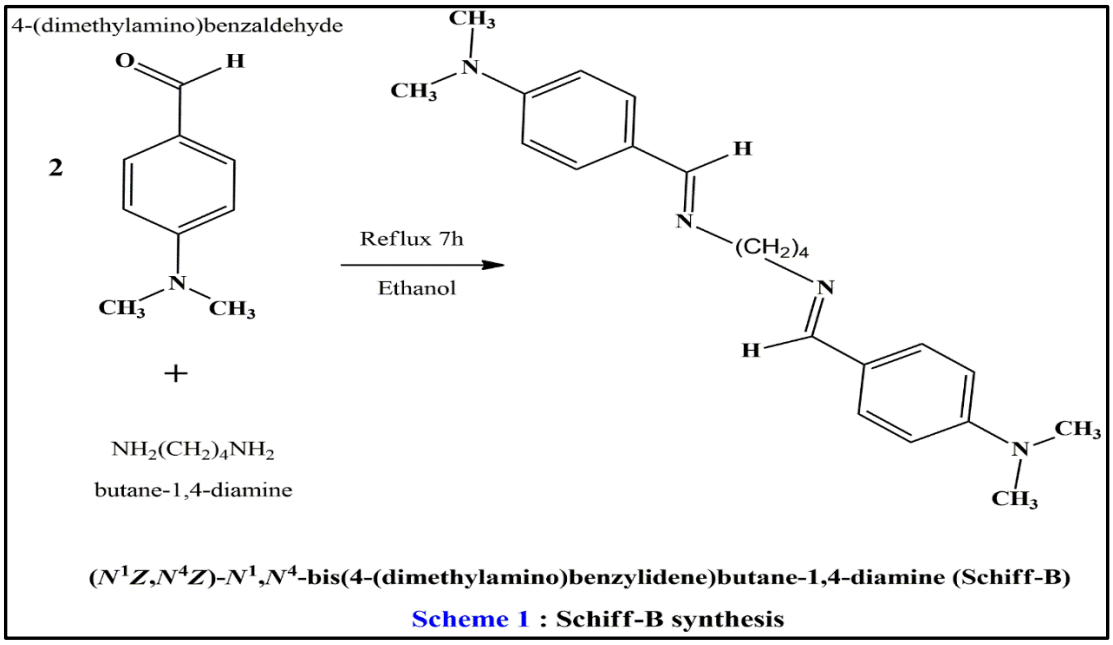

Scheme 1 : Schiff-B synthesis

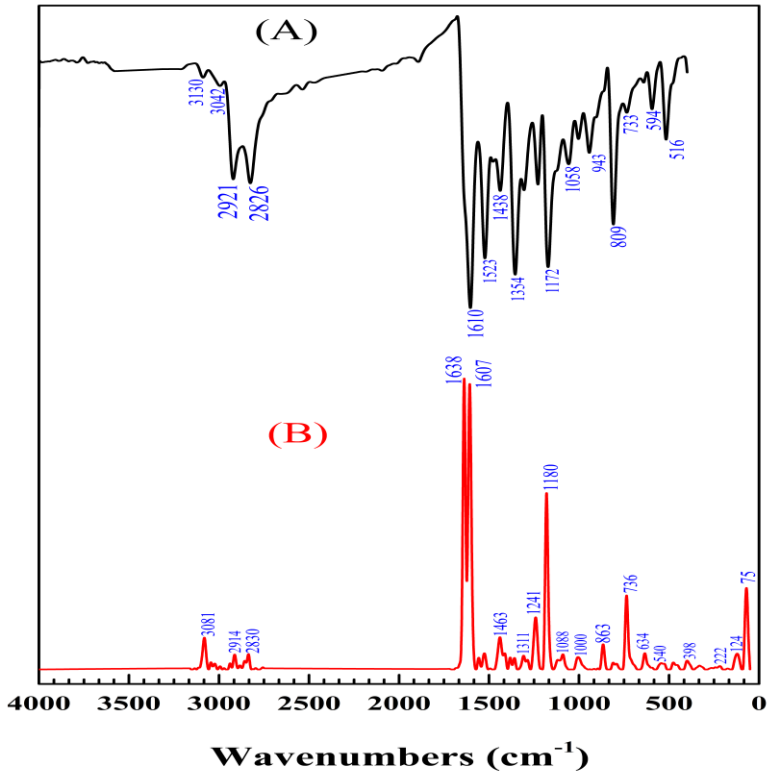

Fig (1): Experimental vibrational spectra of (Schiff-B); (A) IR spectrum given in black colour (4000−500 cm^{-1}) (B) Raman spectrum given in red colour (3500-55 cm^{-1}).

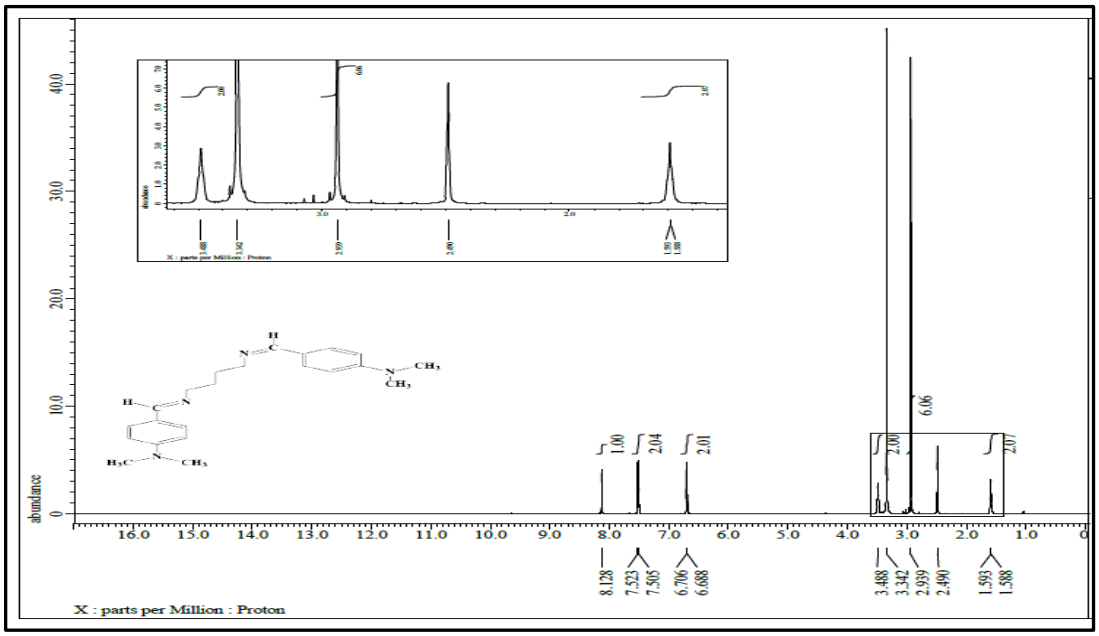

Fig (2): ^{1}HNMR spectrum of Schiff-B

2.4. Spectroscopic Measurements

The Fourier transform infrared (FTIR) spectrum of $C_{22}H_{30}N_4$ from 4000-400 cm^{-1}in the solid state was recorded on Shimadzu FTIR-8300. To acquire the FTIR spectrum (Fig. 1A), 32 accumulative scans were collected at 2 wavenumbers resolution using KBr disk technique. While, the Raman (4000-100 cm^{-1}) spectrum of the finely grinded powdered sample was recorded on Senterra dispersive Raman spectrophotometer (Fig. 1B), Bruker Optics. Laser wavelength of 532 nm, 300 mW, spot size of 1.0 µm, 4 cm^{-1} resolution, 16 scans and 1 sec exposure time. Whereas the proton nuclear magnetic resonance spectrum (^{1}HNMR, Fig. 2) was obtained with the sample dissolved in DMSO-d_6 using 500 MHz Bruker Spectro spin instrument at Ultra Shield magnets, collecting 16 accumulative scans.

3. Computational Part

Due to the capabilities of computers two decades ago, it was difficult to accomplish full optimization for organic compounds with hetero atom(s) by standard *ab initio* calculations at higher levels than the Self-Consistent Field Hartree-Fock (SCF-HF) approach [33]. Recently, the hybrid Density Functional(s) Theory, DFT computations are considered effective and less costly particularly the Becke-Lee-Yang-Parr abbreviated as Becke3LYP functions [34,35] for small, medium and large molecular system [36-38]. On the other hand, the method of Moller Plesset perturbation method to second order (MP2) with and without full electron correlation [39] became less popular owing to high computational cost and incomplete optimizations particularly for large molecular systems [40-43], which is the case for our Schiff B. It worth to mention that, the current computations were limited to our PC specifications (intel Core i7, 10 Gen, 8GB Ram), therefore we could not perform MP2 computations since it fails with more efficient computers [44, 45]. We have performed LCAO-MO-SCF DFT calculations using GAUSSIAN 09 [46] molecular package implementing B3LYP parameters at 6-31+G(d) basis set. For geometry optimization, the energy minima with respect to the nuclear coordinates was obtained by simultaneous relaxation of all geometrical parameters using the gradient method of Pulay [47]. Structure optimization strategies were pursued up to the full convergence criteria in GAUSSIAN 09 (maximum force of 0.000450 mdyne and maximum displacement of 0.001800 Å). Then, the optimized geometry was used to estimate the vibrational frequencies in the harmonic approximation utilizing the same method and basis set. At the optimized local minimum of the potential energy surface (PES), no imaginary frequency was obtained. The results are compared

with earlier computational and vibrational outcomes [48-52] as well as X-ray structural parameters [53, 54] and Electron Diffraction [50].

3.1 Structural Parameters (SPs)

Aided with the published X-ray data [53] of *(N¹Z, N⁴E)-N¹, N⁴*-bis (4 (dimethyl amino) benzylidene) and the available electron diffraction data (ED) of butane 1,4-diamine [55] which contains quartet methylene groups, we were able to compare our theoretical SPs (Table 1) to those obtained experimentally [53], for atom numbering refer to Figure 3C. The estimated (1.091-1.102) and experimental (0.980) values in Å for the C—H_{Me} bond length were in good agreement with variations of 10–11%. Nevertheless, the predicted r(C—H's) of the methylene moiety were ranged from 1.099-1.093 within an average of 0.100±0.003 Å obtained from gas phase ED of n-butane [50, 56]. It is already known that the bond length follows the order: C-$C_{sat.}$ > C⋯C_{ar} > C=C_{ol}. Nevertheless, the aromatic C=C bond length are expected to be conjugated, i.e., an average between pure double bond (1.339-1.340 Å, olefin) and the pure single bond (1.535 Å, Ethan) [57]. Resonance is clearly evidenced herein from the computed CC bond lengths ~ 1.386-1.415 Å. However, (*E*)-4-[(4-Methoxyphenyl) monomethyl] - *N*, *N* dimethyl aniline does not show a clear resonance nearby partial double bond, the r(CC) was found in excellent agreement with those reported earlier (1.531 Å; [50]; 1.533 Å;[52]; 1.547-1.550 Å;[58]; 1.54±0.02; [55]. Our computed values for $C_{10}C_1C_4 \equiv C_1C_4C_7$ were deviated by 0.6°[50]and found within the experimental error [55].

The computed and experimental [53] CNC bond angles were deviated by less than 3%. Nevertheless, the HCH bend angle of methyl and methylene groups were not reported by X-ray and ED studies [50, 52, 55, 58]. Therefore, we have compared them with those obtained for NBenzyl-4-(3-benzyl carbamoyl propyl disulfanyl)- butyramide (BBCPB, $C_{22}H_{28}N_2O_2S_2$) which is a large sized molecules close to Schiff-B (Figure 3B). Since the BBCPB is divided to parts A and B, the reported HCH angle is 109.0(2) and 109.5(11), respectively where the CCH angles were averaged ~110.22±0.15° from ED of n-butane. Nevertheless, the CCCC dihedral angles of benzene rings reveal twisted rings rather than planar, tilted angle ranges ~0.17-0.38° (in-plane) and ~0.37-0.72° (out-of-plane). On the other hand, the τCCCC of ~180, therefore favours *trans* skeletal rearrangements rather than *gauche*.

3.2 Normal coordinate analysis

We have faced technical problems using force constants program like that written by Schacht schneider [59] and modified by Guirgis et al [60] to convert force constants in Cartesian coordinate to that in chosen internal coordinates (F-Matrix). Owing to the relatively large size of the investigated Schiff base and the restrictions on the number of independent internal coordinates that should not exceed eighty, we could not also implement the traditional method suggested by Pulay [47] to calculate B-Matrix using Wilson G.F. method [61]. Therefore, we have used another alternative which have been effectively implemented to carry out NCA [62] using the atomic displacements in x, y and z Cartesian coordinates (ADCC) from B3LYP/6-31+G(d) log file. Selected wavenumbers and their corresponding displacements are illustrated in Figure 4. For simplicity, a conceptual approximation of ADCC were based on omitting 15% of the maximum values either in x, y and/or z directions.

4. Vibrational assignments

The observed infrared (Figure 1A) and Raman (Figure 1B) bands in addition to the computed B3LYP vibrational frequencies along with estimated infrared intensities (km/mol), and Raman scattering activities ($Å^4$ /amu) utilizing 6-31+G(d) basis set (Table 2). Excluding wave numbers below 100 cm^{-1}, the investigated Schiff-B has around 150 active fundamentals in infrared and Raman. Aided by normal coordinate analysis using ADCC, we have provided comprehensive vibrational assignments for most fundamentals regardless of the expected/observed overlapping owing to the large size of the investigated molecule. Moreover, we have also used Gauss View program to visualize normal modes of vibrations whenever appropriate [63].

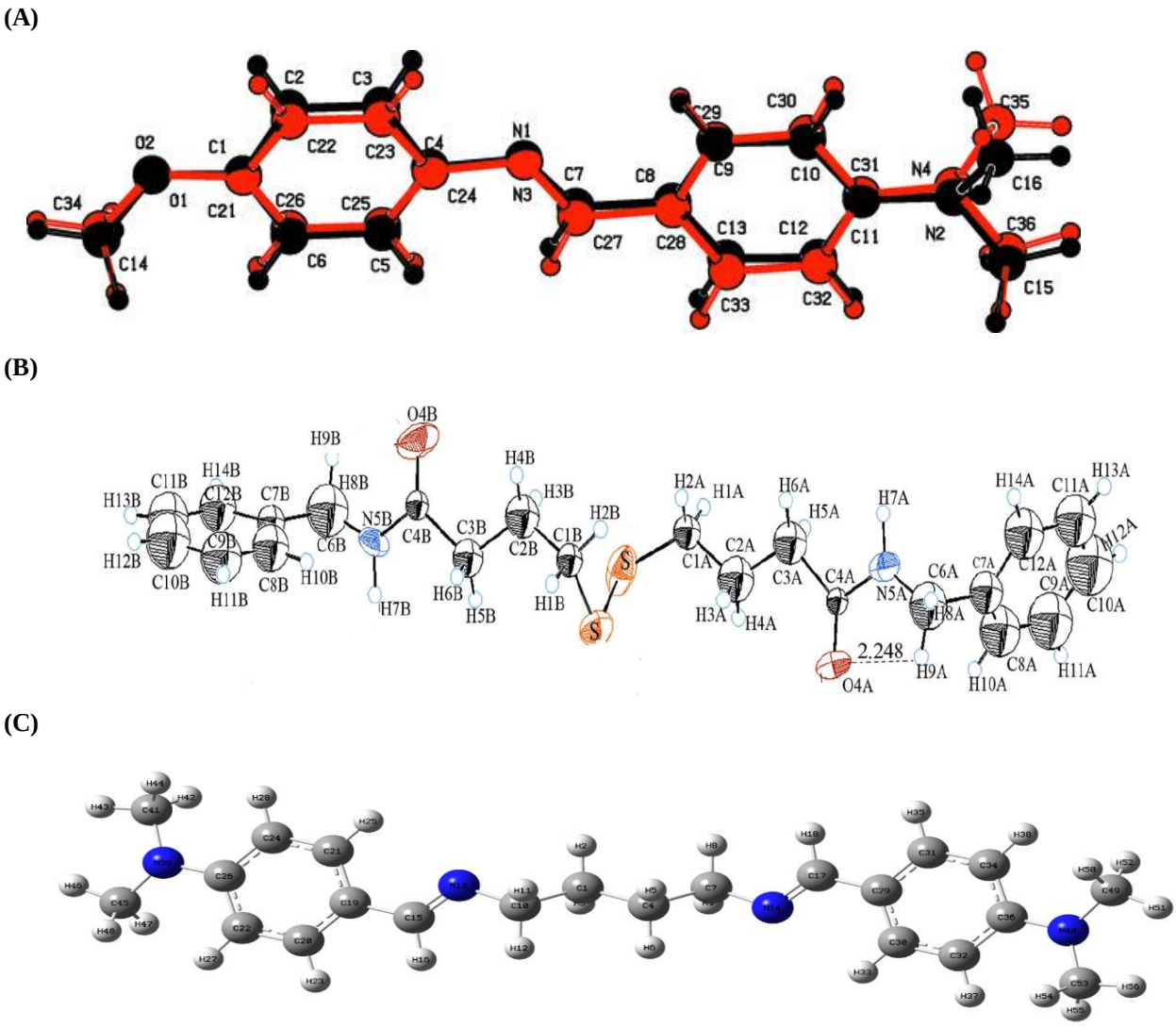

Fig (3): 3Dstructures of (**A**) X-Ray [53]; (B) X-Ray (BBCPB) [54]; (**C**) Optimized Schiff-B

4.1 The 3200−2800 cm^{-1} region

Vibrational spectroscopic feature above 3000 cm^{-1} are expected for C-H aromatic (C-H_{ar}) and olefinic (C-H_{ol}; sp^2) stretches [48, 64, 65]. Therefor the weak IR and medium Raman band observed at 3130 and 3081cm^{-1} is assigned to the overlapped symmetric/asymmetric C-H_{ar} (sp^2) stretches ($\nu_{1\text{-}4}$). The illustrated displacements of hydrogen atoms numbered (H_{25}, H_{27}, H_{28}; ν_3) and (H_{25}, H_{28}; ν_5) is theoretical evidence (Fig. 4). Similar overlapped fundamentals at 3081 cm^{-1} in the Raman spectrum fits the ν_{as} CH_{ar} stretches ($\nu_{5\text{-}8}$) (Figure 1-B and Table 2). Similarly, $\nu_{9\text{-}12}$ are assigned to a sole IR band at 3042 cm^{-1}, however show splitting pattern at 3048, 3021, 2993 and 2970 cm^{-1}, respectively in the Raman spectrum. On the other hand, the C-H unsaturated olefinic bond length (1.105 Å) is predicated longer than those estimated for aromatic (1.088-1.084 Å) and saturated C-H (1.098 Å), thus the $\nu CH_{olefine}$ is observed below 3000 cm^{-1} rather than these commonly reported above 3100 cm^{-1}. A Schiff base with an inversion center is suggested by observing the computed IR intensity and Raman activity of $\nu_{18\text{-}22}$, which reflect the mutual exclusion rule. Nevertheless, we have assumed IR intensities and Raman activities lower than 0.06 Km/mol and 0.4 $Å^4$/amu, of being inactive in both IR and R spectra, respectively. Similarly, ν_{27} ($IR_{int.}$ 222.3 and $R_{act.}$ 0.1; R_{ia}) and ν_{28} ($IR_{int.}$ 0.131; IR_{ia} and $R_{act.}$ 212.3) in

addition to $\nu_{31,32}$;$\nu_{33,34}$;$\nu_{37,38}$;$\nu_{39,40}$;$\nu_{43,44}$;$\nu_{50,51}$;$\nu_{53,54}$;$\nu_{55,56}$;$\nu_{57,58}$;$\nu_{59,60}$;$\nu_{61,62}$;$\nu_{63,64}$;$\nu_{66,67}$;$\nu_{68,69}$;$\nu_{70,71}$;$\nu_{75,76}$;$\nu_{77,78}$;$\nu_{79,80}$;ν_{88},ν_{89};$\nu_{91,92}$;$\nu_{93,94}$;$\nu_{95,96}$;$\nu_{97,98}$;$\nu_{99,100}$;$\nu_{103,104}$;$\nu_{105,106}$;$\nu_{111,112}$;$\nu_{113,114}$;$\nu_{115,116}$;$\nu_{117,118}$;$\nu_{119,120}$;$\nu_{121,122}$;$\nu_{124,125}$;$\nu_{126,127}$;$\nu_{128,129}$;$\nu_{130,131}$;$\nu_{132,133}$;$\nu_{137,138}$;$\nu_{139,140}$;$\nu_{141,142}$;$\nu_{143,144}$;$\nu_{145,146}$;$\nu_{147,148}$. The observed IR bands at 2921 (s) and 2826 (s) covers a range of ~226 cm^{-1} therefore, assigned for overlapped fundamentals ($\nu_{13\text{-}22}$; $\Delta\nu$ = ±55cm^{-1}) that fit the unresolved strong IR band at 2921 cm^{-1}, other saturated, olefin and aromatic CH stretches are given in Table 2. Identical wavenumbers ($\nu_{9\text{-}26}$) from 3150-2947 cm^{-1} match νC-H_{alkane} (sp^3; CH_3 and CH_2) while the νC-$H_{olefinic}$ (sp^2) were estimated at 2970 cm^{-1}. It is worth mentioning that unscaled wavenumber ~3229-3200 cm^{-1} was scaled herein ~3132-3104 cm^{-1}.

4.2 The 1700−1000 cm^{-1} region

According to earlier spectral observations [17, 22, 48], the reported C=N and/or C=C stretches are favoured to the very strong IR band at 1610 cm^{-1} and the split Raman bands at 1638 and 1607 cm^{-1}, respectively. The symmetric (ν_{31}; IR_{ia}& R_a) and antisymmetric (ν_{32}; IR_a& R_{ia}) C=N stretches are assigned to very strong bands observed at 1638 (R) and 1610 (IR) cm^{-1}, respectively. While the Raman band 1607 cm^{-1} (vs) favors C=C quadrant aromatic stretch as suggested by Colthup et al [48] in agreement with split Raman bands at 1588 and 1563 cm^{-1}[66]and ~1563-1612 cm^{-1} [22]. The C=N stretch was ranged from 1649-1599 cm^{-1}in IR and matrix isolated infrared spectra of 2-(N-phenyliminomethyl)–phenol,2-(Nmethyliminomethyl)-phenol, 2-(N-methyl-α-iminoethyl)-phenol, 2-(N-methyl-α-iminoethyl)-4-chlor-6-nitrophenol and 2-(N-methyl-α-iminoethyl)-4, 6-dichlorophenol Schiff bases [17]. The $\nu_{33\text{-}36}$ were unscaled/scaled at 1626/1660 cm^{-1}, thus assigned to C=C_{ar} stretches in which $\nu_{33,}\nu_{35}$ is Raman active (R_a) and almost IR inactive (IR_{ia}), therefore observed at 1607 cm^{-1} (vs) in the Raman spectrum [67]. On the other hand, the observed IR band at 1523 cm^{-1} (vs) fits $\nu_{37,38}$ fundamentals without Raman analogs, Moreover, ν_{34}, ν_{36} is presumably Raman inactive (calc. Raman activity of ~ 03 $Å^4$/amu) but infrared active (894 Km/mol), it is observed herein at 1523 cm^{-1} (vs). It is worth to mention that ν_{31} and ν_{33} fundamentals have the highest Raman scattering activities of 3307 and 3210 units $Å^4$/amu, respectively whereas ν_{32} and ν_{34} have the highest IR activities of 363- and 894-units km/mol, respectively.

The δCH_{ar}, $\delta_{Sciss}CH_2$ and δCH_3 ($\nu_{37\text{-}46}$) are unscaled from 1570-1516 cm^{-1} ($\Delta\nu$ = 50 cm^{-1}) theoretically separated by 4 cm^{-1} (Table 2), hence assigned for the observed IR and R bands at 1463 cm^{-1}. However, the combined weak Raman bands at 1438 and 1421 cm^{-1} and the strong/shoulder IR bands at 1463 cm^{-1} and 1438 cm^{-1} agree with $\nu_{39\text{-}46}$ and$\nu_{47\text{-}52}$, respectively. As the matter of fact, the other δ_{as} CH_3 (ν_{41}, ν_{42}) and $\delta_{sciss.}CH_2$($\nu_{43,44,47,50}$) were separated by 35 cm^{-1}, assigned to the weak Raman band at 1421 cm^{-1}, however ν_{47} has the highest Raman activity (58.6 $Å^4$/amu) among ν_{41}-ν_{52}(Table 2). Likewise, the counterpart IR band observed at 1438 cm^{-1} has the highest $IR_{int.}$ (85.5 Km/mole) among ν_{41}-ν_{52} fundamentals. Noticeably, the CH_2/CH_3 bending modes including scissors, umbrella, antisymmetric ($\nu_{47\text{-}52}$) are theoretically separated by 4 cm^{-1}(Table 2), thus the measured in IR/R bands at 1438/1421 cm^{-1} are within ~ 1544-1504 cm^{-1}[17], hence fit $\nu_{47\text{-}52}$ fundamentals. The observed IR band at 1354 cm^{-1} (vs) fits the ν CC ar (ν_{53}, ν_{54}), δ_{um} CH_3 (ν_{55}, ν_{56}), δ_{ip}C-H_{ol} (ν_{57}, ν_{58}), and δ_{wag} CH_2 (ν_{59}, ν_{60}) in agreement with calculated infrared intensities (645.3 km/mol) and were unscaled/scaled around (1479-1400)/(1419-1400) cm^{-1}, where $\Delta\nu$ is 19 cm^{-1}. While the weak resolved Raman bands at 1409, 1379, 1353 and 1340 cm^{-1} were interpreted CC_{ar} stretches (Table 2). Nevertheless, the νCC_{ar} observed at 1409 cm^{-1} named as semi-circle stretch [48]is well compared to those reported earlier at 1418 cm^{-1}[66]and 1410 cm^{-1}[68]. Hence, the conjugated C=C stretches ($\nu_{53,54,63,64}$) is red shifted and observed from 1409-1311 cm^{-1} regardless of their mixing/overlapping (Table 2).

The νC=N, ν C=C_{ar}, δCH_2 (wag, twist) and δ_{ip} CH_{ar} ($\nu_{61\text{-}70}$) fundamentals differs only by 28 cm^{-1}; hence, could match 1300/1311 cm^{-1} (IR/R). Nevertheless, the Raman counterpart is accompanied with a shoulder at low frequency side ~1286 cm^{-1} (Table 2**)**. $\delta CH_{(ip)}$ (ν_{66}, $\nu_{67,}$ ν_{75}), νC-N_{Me} (ν_{71}, $\nu_{72,}$), δ_{wag} CH_2 ($\nu_{73,}$ ν_{74}) and δ_{twist} CH_2 (ν_{68}, $\nu_{69,}$ ν_{70}) modes were separated by $\Delta\nu$ ± 80 cm^{-1} thus fundamentals ($\nu_{66,67}$) are assigned for IR/Raman bands at 1300/1311 cm^{-1} while $\nu_{71,72,75}$ match those recorded at 1234(s)/1241(m) cm^{-1}, in agreement with the predicted $IR_{int.}$ and $R_{act.}$ (Table 2). The methyl and

methylene bending modes were found in close vicinity to those reported earlier for organic molecules [48, 49, 64, 69], with emphasis on δCH_2~1419/1464 ($\delta_{Scissor}$),~1280/1276 (γ), ~1300/1302 (δ_{twist}) for di-n-butyl ether which contains quartet CH_2 moieties [64].

Nevertheless, ρCH_3 was reported at ~1093/1093 cm^{-1} (R/IR) for dimethylformamide nearby those given by Durig et al for n-butane [51]. While the observed $\delta_{ip}CH$ bending modes ~1523-1117 and ~809-1088 cm^{-1} were in good match within ±50 cm^{-1} compared to References [17, 70]~1490-1159 cm^{-1} and ~895-1003 cm^{-1}, respectively.

The following fundamentals between (1200-895 cm^{-1}) are characterized by extensive overlapping and mixing. Because of ±17 cm^{-1} separation (ν_{76-80}), the observed Raman/IR band at 1180(s)1172(vs) cm^{-1} fit $\delta_{(ip)}CH_{ar}$, $\delta_t CH_2$ and ρ CH_3 modes.

Similarly, ν_{81-87} were overlapped which fit wavenumbers at 1117sh (IR)/1088s(R) cm^{-1} and found dominated by ρ $CH_{2\ (rocking)}$, δ_{ip} CH aromatic and ρ CH_3 modes. Following the same consent, ν_{88-93} were assigned to ρ CH_3 ($\nu_{89,90}$), ν C-N (ν_{93}) and ν CC (ν_{92}) fit an IR a shoulder at 1058 cm^{-1}within ~1022-1012 cm^{-1} given by Smith et al [22].

Indeed, ν_{92} and ν_{93} normal modes were identical at 1064/1058 cm^{-1} (calculated/observed). It is worth mentioning that the CH_{ar} and CH_{ol} were expected within 980-1025 cm^{-1} ($\Delta\nu$±45cm^{-1}) as per B3LYP theoretical predictions, therefore the IR_a/R_a fundamentals ($\nu_{94,95,98,99}$/ $\nu_{96,97,100}$) were assigned to IR/R bands at 1003/1000 cm^{-1}, in agreement with the estimated IR_{int} and R_{act} (Table 2).

The observed band at 943 cm^{-1} in both IR and Raman spectra is assigned to CN stretches ($\nu_{101,102}$) [38, 39]. The ($\nu_{103,105}$) are R_{ia}, but ν_{104} is R_a with low R_{act} (5.0 $Å^4$/amu), therefore barely observed at 914 cm^{-1}. These overlapped fundamentals $\nu_{103-105}$ were estimated to be weak (IR_{int}; 2.9 Km/mol), observed at 900/914, 895cm^{-1} (IR/R); (Figure 1-A, B and Table 2). It is noted that the dominant γCH_{ar} (ν_{105}; $H_{23,27,35,38}$) is mixed with both γCH_{ol} ($H_{16,18}$) and ρCH_2 ($H_{2,3,5,6}$) owing to the large ADCC (Fig4C) of the involved atoms (Fig. 3C for atom numbering).

4.3 The 900−75 cm^{-1} region

The ring breathing (ν_{106}; R_a /ν_{107}; IR_a) was adjusted straightforward to the observed bands at 863 (w, sh) and 868 cm^{-1} (m) in the Raman and IR spectra, respectively. The band at 809 cm^{-1} were assigned to the *out-of-plane* ring deformation (δ_{oop}; ν_{108}-ν_{111}).

While the IR_a modes, ν_{113} (ρ CH_2) andν_{115} (δ_{oop} ring twist) fit an IR shoulder at 733 cm^{-1} (m). Moreover, ν_{114} andν_{117} fit the strong Raman band at 736 cm^{-1} (m) which is dominated by ring bending modes.

The spilt Raman band centered at 634 cm^{-1} (m) favours ν_{119} (~605-635 cm^{-1}). On the other hand, the IR band at 594 cm^{-1} was adjusted to ν_{120}. ν_{122}, ν_{124} and ν_{126} fundamentals and that recorded at 516 cm^{-1} (m) is dominated by δ_{ring} CCC plus minor ρ CH_3. Mixed *in-planning* (ν_{120}) and outer ring (C_rNC_{Me}) bending modes (ν_{125}) is observed at 476 cm^{-1} (R, sh), overlapped with $C_{22}C_{26}N_{Me}$; unscaled at 486 cm^{-1} which is verified by the large ADCC of the assigned atoms, C_{41}, N_{39}, C_{45} and C_{26} and nearby atoms. Another mixing is found in δ C-C-N, δ C-N=C and δ C-C-C_{al} that recorded/calculated at 451/448 cm^{-1} (ν_{128}) compared to Raman band at 432 cm^{-1} for n-butane.

The observed vw Raman features at 247 and 266 cm^{-1} were assigned to overlapped Me torsions while those recorded at 222 cm^{-1} reflects both γ C=N-C and γ N=C-C *out-of-plane* mixed with minor methyl torsion. Approximate description of selected fundamentals was given below (Fig. 4A-C).

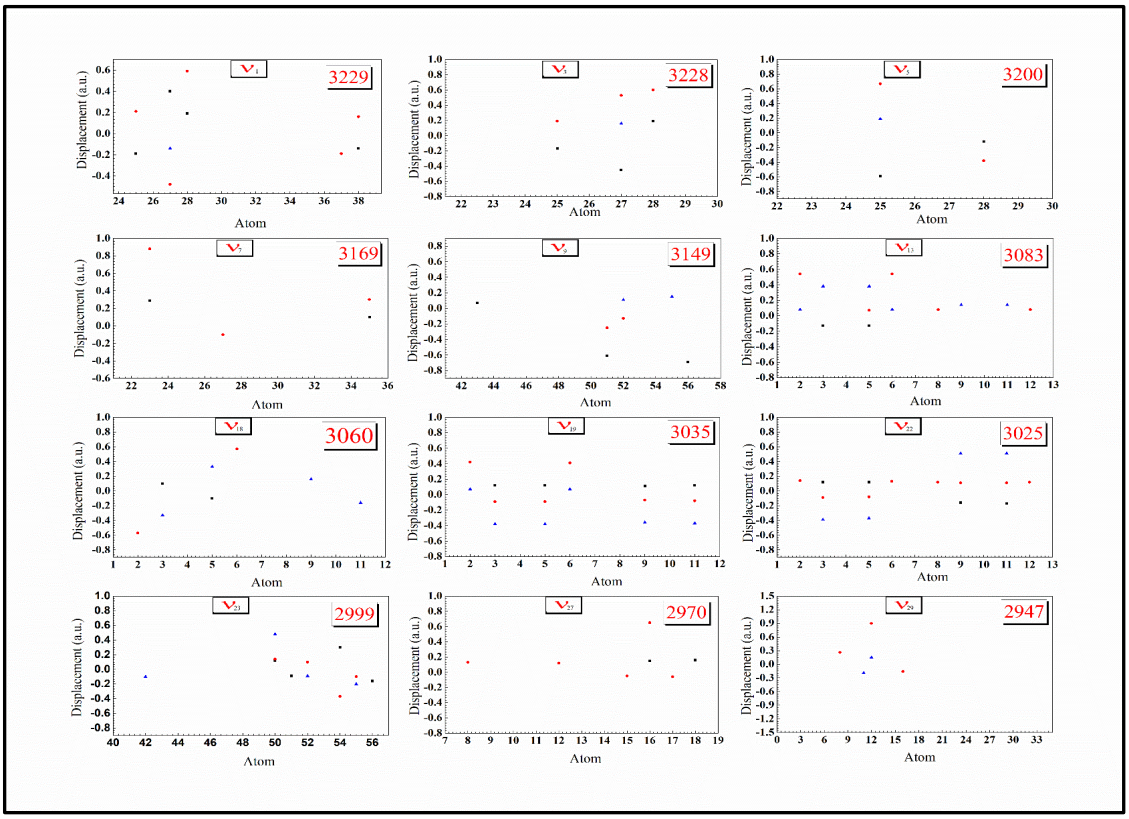

Fig (4A): Cartesian coordinate displacements of the normal vibrations of the prepared Schiff-B.

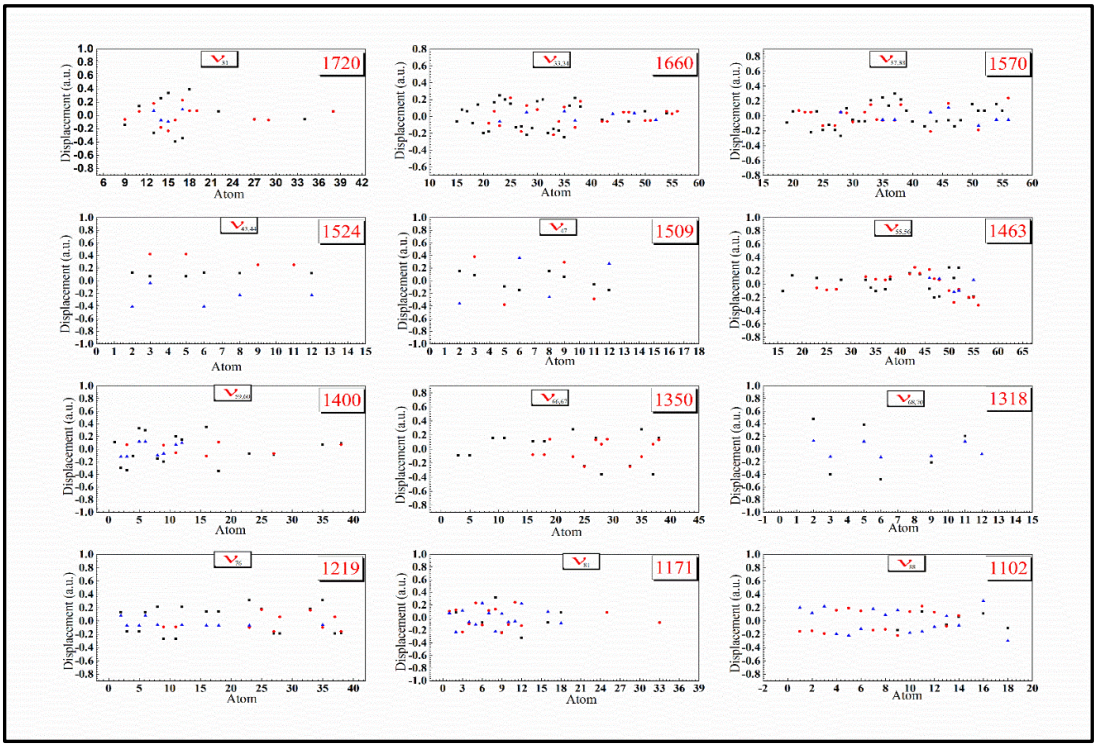

Fig (4B): Cartesian coordinate displacements of the normal vibrations of the prepared Schiff-B.

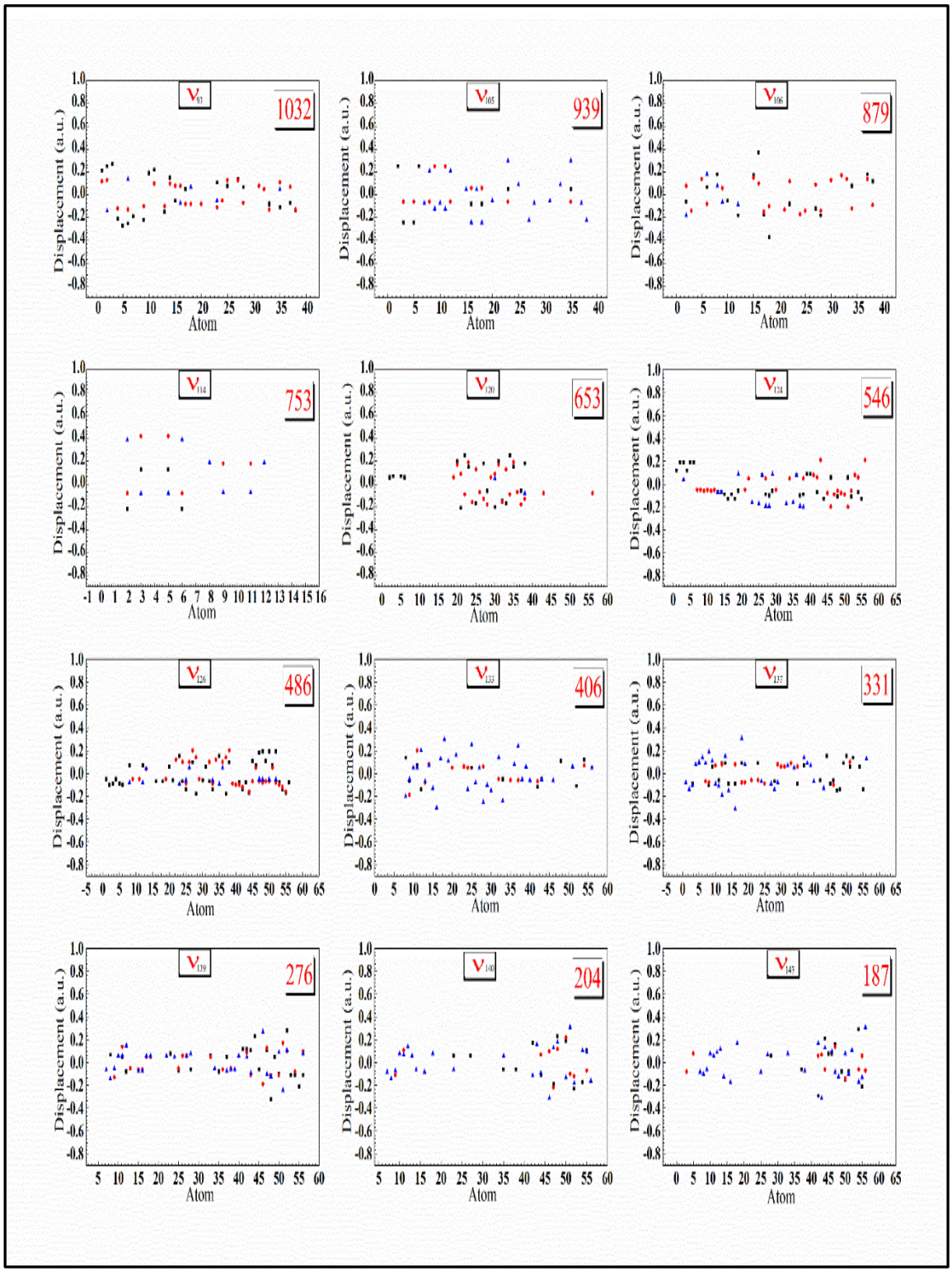

Fig (4C): Cartesian coordinate displacements of the normal vibrations of the prepared Schiff-B.

Table 1: Calculated structural parameters[a] for the investigated Schiff-B inhibitor [b]

Structural Parameters [a]	*X-ray* [53]	*X-ray* [54]	*Electron diffraction* [50]	*B3LYP/ 6-31+G(d)*
		Bond length (r)		
r (C_{45}—H_{47}) Me	0.9800	-	-	1.102
r (C_{45}—H_{48}) Me	0.9800	-	-	1.096
r (C_{45}—H_{46}) Me	0.9800	-	-	1.091
r (C_{41}—H_{43}) Me	0.9800	-	-	1.091
r (C_{41s}—H_{44}) Me	0.9800	-	-	1.096
r (C_{41}—H_{42}) Me	0.9800	-	-	1.102
r (C_{45}—N_{39}) Me	1.4502	-	-	1.454
r (C_{41}—N_{39}) Me	1.4455	-	-	1.455
r (C_{26}—N_{39}) Me	1.3826	-	-	1.386
r (C_{15}—C_{19})	1.4534	1.52(3)	-	1.466
r (C_{21}=C_{19}))≡(C_{29}=C_{30})	1.3899	1.38(2)	-	1.406
r (C_{19}=C_{20})≡(C_{29}=C_{31})	1.4028	1.40(2)	-	1.402
r (C_{20}=C_{22})≡(C_{31}=C_{34})	1.3721	1.42(2)	-	1.391
r (C_{22}=C_{26})≡(C_{34}=C_{36})	1.4112	1.44(3)	-	1.415
r (C_{26}=C_{24})≡(C_{36}=C_{32})	1.4048	1.37(2)	-	1.420
r (C_{24}=C_{21})≡(C_{31}=C_{30})	1.3790	1.34(2)	-	1.386
r (C_{15}—H_{16})	0.9500	-	-	1.105
r (C_{20}—H_{23})	0.9500	-	-	1.088
r (C_{22}—H_{27})	0.9500	-	-	1.083
r (C_{24}—H_{28})	0.9500	-	-	1.083
r (C_{21}—H_{25})	0.9500	-	-	1.086
r (N_{13}=C_{15})	1.272	-	-	1.27
r (N_{13}—C_{10})	1.412	1.40(2)	-	1.452
r (C_1—C_4)	-	1.47(2)	1.531	1.533
r (C_1—C_{10})	-	1.57(2)	1.531	1.535
r (C_4—C_7)	-	1.49(2)	1.531	1.535
r (C—H) CH2	-	-	1.119	1.099-1.093
		***Bond (∠) and dihedral angles* (τ)**		
∠($C_{15}N_{13}C_{10}$)≡($C_{17}N_{14}C_7$)	121.70	-	-	118.3
∠ ($C_{45}N_{39}C_{26}$)≡($C_{49}N_{40}C_{36}$)	119.93	-	-	119.5
∠ ($C_{45}N_{39}C_{41}$)≡($C_{53}N_{40}C_{49}$)	115.71	-	-	118.1
∠ ($C_{41}N_{39}C_{26}$)≡($C_{53}N_{40}C_{36}$)	119.71	-	-	119.6
∠ ($H_3C_1H_2$) CH2	-	109.5(11)/ 109.0(2)	-	106.5
∠ ($H_5C_4H_6$) CH2	-		-	106.5
∠ ($H_9C_7H_8$) CH2	-		-	107.3
∠ ($H_{12}C_{10}H_{11}$) CH2	-		-	107.3

Table 1: Continued.

Structural Parameters [a]	*X-ray* [53]	*X-ray* [54]	*Electron diffraction* [50]	*B3LYP/ 6-31+G(d)*
∠ ($H_{47}C_{45}H_{46}$) $_{Me}$	110.00	-	-	108.3
∠ ($C_{10}C_1C_4$)≡($C_1C_4C_7$) $_{CH2}$	-	119.0(2)	113.3	112.7
∠ ($N_{39}C_{45}H_{48}$)	109.00	-	-	111.0
∠ ($N_{39}C_{45}H_{47}$)	109.00	-	-	112.6
∠ ($N_{39}C_{45}H_{46}$)	109.00	-	-	109.1
∠ ($H_{48}C_{45}H_{47}$)	109.00	-	-	108.2
∠ ($C_{19}C_{15}N_{13}$)	122.55	117.0(2)	-	124.0
∠ ($C_{20}C_{19}C_{15}$)	122.50	-	-	120.2
∠ ($C_{21}C_{19}C_{15}$)	120.38	122.0(2)	-	122.3
∠ ($C_{21}C_{19}C_{20}$)	117.09	-	-	117.5
∠ ($C_{19}C_{20}C_{22}$)	121.81	121.0(2)	-	121.9
∠ ($C_{20}C_{22}C_{26}$)	120.98	123.0(2)	-	120.8
∠ ($C_{24}C_{26}N_{39}$)	121.46	-	-	121.3
∠ ($C_{22}C_{26}C_{24}$)	117.17	115.0(2)	-	117.2
∠ ($C_{22}C_{26}N_{39}$)	121.35	-	-	121.5
∠ ($C_{26}C_{24}C_{21}$)	120.97	121.0(2)	-	121.2
∠ ($C_{24}C_{21}C_{19}$)	121.97	124.0(2)	-	121.4
∠ ($C_{19}C_{15}C_{16}$)	119.00	-	-	115.1
∠ ($H_{16}C_{15}N_{13}$)	119.00	-	-	120.9
∠ ($H_{23}C_{20}H_{19}$)	119.00	-	-	119.4
∠ ($C_{22}C_{20}H_{23}$)	119.00	120.0(2)	-	118.8
∠ ($C_{26}C_{22}H_{27}$)	119.00	116.0(2)	-	120.6
∠ ($C_{20}C_{22}H_{27}$)	120.00	-	-	118.7
∠ ($C_{21}C_{24}H_{28}$)	119.00	120.0(2)	-	118.5
∠ ($C_{26}C_{24}H_{28}$)	120.00	-	-	120.3
∠ ($C_{19}C_{21}H_{25}$)	119.00	118.0(2)	-	118.6
∠ ($C_{24}C_{21}H_{25}$)	119.00	-	-	119.9
∠ ($H_{43}C_{41}N_{39}$)	109.00	-	-	109.0
∠ ($H_{42}C_{41}H_{44}$)	109.00	-	-	108.2
∠ ($H_{42}C_{41}H_{43}$)	109.00	-	-	108.3
∠ ($H_{42}C_{41}N_{39}$)	109.00	-	-	112.6
∠ ($H_{44}C_{41}N_{39}$)	109.00	-	-	111.1
∠ ($H_{43}C_{41}H_{44}$)	109.00	-	-	107.5
∠ ($H_{48}C_{45}H_{46}$)	110.00	-	-	107.5
τ ($C_{10}N_{13}C_{15}C_{19}$)	-177.55		-	-179.9
τ ($C_{21}C_{19}C_{20}C_{22}$)	-0.17		-	-0.22

Table 1: **Continued.**

Structural Parameters [a]	*X-ray* [53]	*X-ray* [54]	*Electron diffraction* [50]	*B3LYP/ 6-31+G(d)*
τ ($C_{19}C_{20}C_{22}C_{26}$)	-0.38	3.0(2)/ -1.0(2)	-	-0.44
τ ($C_{20}C_{22}C_{26}C_{24}$)	0.72	-4.0(2)/ 0.0(3)	-	1.09
τ ($C_{21}C_{24}C_{26}N_{39}$)	179.19	-	-	178.4
τ ($C_{15}C_{19}C_{20}C_{22}$)	-177.57	178.0(3)	-	-179.9
τ ($N_{39}C_{26}C_{22}C_{20}$)	-179.00	-	-	-178.4
τ ($C_{45}N_{39}C_{26}C_{24}$)	175.35	-	-	171.1
τ ($C_{41}N_{39}C_{26}C_{22}$)	-161.06	-	-	-170.03
τ ($C_{45}N_{39}C_{26}C_{22}$)	-6.25	-	-	-9.37
τ ($C_{41}N_{39}C_{26}C_{24}$)	20.54	-	-	10.44
τ ($N_{13}C_{15}C_{19}C_{21}$)	-1.15	-	-	0.33
τ ($N_{13}C_{15}C_{19}C_{20}$)	176.68	161.0(3)	-	180
τ ($C_{15}C_{19}C_{21}C_{24}$)	177.73	-179.0(4)	-	179.9
τ ($C_{22}C_{26}C_{24}C_{21}$)	-0.52	-1.0(3)	-	-1.10
τ ($C_{26}C_{22}C_{20}C_{19}$)	-0.02	-1.0(2)	-	-0.44

[a] Bond distances (r) in angstroms, bond (∠) and dihedral angles (τ) in degrees.

[b] The X-ray structure of (N1Z, N4E)-N1, N4-bis (4-(dimethyl amino) benzylidene) butane-1,4-diamine (Schiff-B).

Table 2: Observed and calculated (B3LYP) frequencies (cm^{-1}) for the investigated Schiff-B inhibitor.

υ_i	*Fundamental*[a]	*B3LYP/6-31+G(d)*				*Obs. (this study)*[d]	
		Unscaled	***Fixed Scal.***	***IR Int.***[b]	***Raman act.***[c]	***IR solid***	***Raman***
υ_1	ν_s/ν_{as} $CH_{aromatic}$	3228	3132	6.02	285	(3130w)	-
υ_2				24.2	72.1		
υ_3				20.3	30.4		
υ_4				16.5	37.1		
υ_5	ν_{as} $CH_{ar.}$	3200	3104	1.7	36.7	-	(3081m)
υ_6				2.1	30.3		
υ_7	ν_{as} $CH_{ar.}$	3169	3074	26.1	26.2		
υ_8				6.2	110		
υ_9	ν_s (CH_3)	3149	3054	40.4	296	(3042vw)	3048w
υ_{10}				61.2	195		3021w
υ_{11}	ν_{as} (CH_3)	3137	3043	2.1	2.9		2993vw
υ_{12}				2.1	3.0		2970vw
υ_{13}	ν_{as} (CH_2)	3083	2987	81.5	Ia	(2921s)	-
υ_{14}	ν_{as} (CH_3)	3072	2979	48.9	96.6	(2921s)	2938sh,vw
υ_{15}				50.4	94.5		(2914w)
υ_{16}				30.9	121		
υ_{17}				31.1	120		
υ_{18}	ν_{as} (CH_2)	3060	2968	ia	60.7	-	2914w
υ_{19}	ν_s/ν_{as} (CH_2)	3035	2944	97.1	Ia	(2921s)	-
υ_{20}				ia	301	-	2866sh,vw
υ_{21}				17.5	0.01	(2921s)	-
υ_{22}	ν_s (CH_2)	3025	2934	ia	383	-	2866sh,vw
υ_{23}	ν_s (CH_3)	3000-2991	2910	80.5	403	(2826s)	(2830w)
υ_{24}				160	203		
υ_{25}				91.4	125		
υ_{26}				86.1	132		
υ_{27}	ν_{as} $(CH_{olefine})_{N=C-H}$	2970	2881	222	0.1	2826s	-
υ_{28}	ν_s $(CH_{ol.})_{N=C-H}$			0.131	212	-	2830w
υ_{29}	ν_s (CH_2)	2947	2858	103.9	63.8	2826s	-
υ_{30}				31.4	211	-	
υ_{31}	ν_s (C=N)	1720	1685	ia	3307	-	1638vs
υ_{32}	ν_{as} (C=N)	1718	1683	362.7	0.01	(1610vs)	
υ_{33}	ν $C=C_{ar.}$	1660	1626	0.01	3210	(1610vs)	(1607vs) 1577w
υ_{34}				894	0.02		
υ_{35}				2.1	155		
υ_{36}				69	4.8		
υ_{37}	δ_{ip} $CH_{ar.}$	1570	1507	1.3	152	1523vs	(1528w)
υ_{38}				373	0.5		
υ_{39}	δ_{as} CH_3	1540	1478	0.05	80.0	(1463sh,w)	(1463m)
υ_{40}				96.3	Ia		
υ_{41}				3.5	6.6		
υ_{42}				4.2	5.6		

Table 2: **Continued.**

v_i	*Fundamental*[a]	*B3LYP/6-31+G(d)*				*Obs. (this study)*[d]	
		Unscaled	*Fixed Scal.*	*IR Int.*[b]	*Raman act.*[c]	IR_{solid}	*Raman*
v_{43}	δ Sciss CH_2	1524	1463	15.2	*Ia*	(1463sh,w)	(1463m)
v_{44}				*ia*	38.1		
v_{45}	δ_{as} CH_3	1516	1455	13.9	32.3		
v_{46}				15.5	28.9		
v_{47}	δ Sciss CH_2	1509	1448	*ia*	58.6	(1438s)	(1421w)
v_{48}	δ_{as} CH_3	1508	1447	4.1	3.8		
v_{49}				1.7	9.1		
v_{50}	δ Sciss CH_2	1506	1445	9.6	*Ia*		
v_{51}	δ_s CH_3 (umbrella)	1505	1444	0.3	20.9		
v_{52}				85.5	0.07		
v_{53}	ν $CC_{ar.ring}$	1479	1419	1.3	64.3	(1354vs)	(1409sh,w)
v_{54}				31.7	2.7		
v_{55}	δ_s CH_3 (umbrella)	1463	1404	0.2	83.8		(1379w)
v_{56}				16.3	1.2		
v_{57}	δ_{ip} C-$H_{ol.}$	1426	1369	0.1	118		1353w
v_{58}				13.4	0.8		-
v_{59}	δ wag (γ) CH_2	1400	1400	*ia*	79.9		1340w
v_{60}				23.7	*Ia*		-
v_{61}	ν C-N	1390	1362	3.0	135	(1300sh,s)	(1311w) 1286sh,w
v_{62}				645	0.6		
v_{63}	ν $CC_{ar.r}$	1372	1344	2.6	5.5		
v_{64}				32.8	0.4		
v_{65}	δ wag (γ) CH_2	1362	1362	*ia*	14.0		
v_{66}	$\delta_{ip}CH_{ar.}$	1350	1296	130	*Ia*		
v_{67}				*ia*	212		
v_{68}	δ_t CH_2	1318	1265	2.1	*Ia*		
v_{69}				*ia*	64.5		
v_{70}				*ia*	171		
v_{71}	ν $(C\text{-}N)_{Me}$	1277	1226	63.8	3.8	(1234s)	(1241m)
v_{72}				3.4	74.1		
v_{73}	δ wag (γ) CH_2	1272	1227	9.9	0.2		
v_{74}				33.8	0.01		
v_{75}	$\delta_{ip}CH_{ar.}$	1271	1220	*ia*	296		
v_{76}	δ_tCH_2	1219	1170	225	0.01	(1172vs)	(1180s)
v_{77}	$\delta_{ip}CH_{ar.}$	1217	1168	*ia*	616.5		
v_{78}	δ_t CH_2	1211	1162	46.5	*Ia*		
v_{79}	ρ CH_3 (rocking)	1202	1145	0.1	17.4		
v_{80}				69.1	0.04		
v_{81}	ρ CH_2 (rocking)	1171	1124	*ia*	1.2	(1117sh,w)	(1088w)
v_{82}	$\delta_{ip}CH_{ar.}$	1160	1113	0.7	1.4		
v_{83}				0.7	1.5		

Table 2: Continued.

υ_i	Fundamental[a]	B3LYP/6-31+G(d)				Obs. (this study)[d]	
		Unscaled	Fixed Scal.	IR Int.[b]	Raman act.[c]	IR_{solid}	Raman
υ_{84}	ρ CH_3 (rocking)	1150	1104	12.0	55.3	(1117sh,w)	(1088w)
υ_{85}				107.5	5.7		
υ_{86}				0.8	1.7		
υ_{87}				0.8	1.7		
υ_{88}	ν $CC_{aliphatic}$	1102	1058	*ia*	30.0	(1058sh,m)	-
υ_{89}	ρ CH_3 (rocking)	1088	1044	45.5	0.03		
υ_{90}				2.0	0.6		
υ_{91}	ν C-N + ν $CC_{al.}$	1064	1011-1042	64.2	*Ia*		
υ_{92}	ν $CC_{al.}$	1062		*ia*	52.0		
υ_{93}	ν C-N + ν $CC_{al.}$	1032		*ia*	106.1		
υ_{94}	δ_{oop} C-$H_{ol.}$	1025	984	18.8	*Ia*	(1003w)	(1000w)
υ_{95}		1022	981	1.4	*ia*		
υ_{96}				*ia*	21.6		
υ_{97}		999	959	*ia*	21.0		
υ_{98}	$\delta_{oop}CH_{ar.}$	995-980	955-940	13.6	*ia*	(1003w)	(1000w)
υ_{99}				1.1	*ia*		
υ_{100}				*ia*	9.4		
υ_{101}	ν C-N_{Me} + δ_{ip} ring def	966	946	19.2	18.8	(943m)	943vvw
υ_{102}				40.0	9.0		
υ_{103}	ρ CH_2 (rocking) + $\delta_{oop}CH_{ar.}$	953	914	1.7	*ia*	-	914vvw 895vvw
υ_{104}	$\delta_{oop}CH_{ar.}$	946-939	908-901	*ia*	5.0		
υ_{105}				2.9	*ia*		
υ_{106}	ν_s C=C ring breathing	879-869	851-844	*ia*	30.5	868sh,w	863m
υ_{107}				4.9	*ia*		
υ_{108}	$\delta_{oop}CH_{ar.}$	833-810	799-777	52.4	0.4	809s	(809w)
υ_{109}				45.0	0.4		
υ_{110}	ρ CH_2 + ν_s C=C ring breathing			*ia*	4.1		
υ_{111}				18.6	*ia*		
υ_{112}	ρ CH_2 (rocking)	753-734	732-704	*ia*	6.7	(733sh,m)	(736s)
υ_{113}				5.3	*ia*		
υ_{114}	δ_{oop} ring def			*ia*	59.7		
υ_{115}				6.0	*ia*		
υ_{116}				1.2	*ia*		
υ_{117}				*ia*	5.0		
υ_{118}	δ_{ip} ring def	605-653	580-626	2.2	*ia*	594m	634m
υ_{119}				*ia*	12.6		
υ_{120}				25.9	*ia*		
υ_{121}				*ia*	0.5		
υ_{122}	δ_{oop} ring def	534-547	512-525	3.0	*ia*	(516m)	540w
υ_{123}				*ia*	0.4		
υ_{124}				37.0	*Ia*		

Table 2: Continued.

υ_i	Fundamental[a]	B3LYP/6-31+G(d)				Obs. (this study)[d]	
		Unscaled	Fixed Scal.	IR Int.[b]	Raman act.[c]	IR_{solid}	Raman
υ_{125}	δ_{ip} ring def. + δC_rNC_{Me}	480-506	460-485	*Ia*	4.2	(516m)	476sh,w
υ_{126}				11.5	*ia*		
υ_{127}	$\delta C_{22}C_{26}N_{39}$			*Ia*	5.1		
υ_{128}	δ CCN + δ C-N=C+ $\delta CCC_{alchain}$	448	448	*Ia*	3.6		451sh,vw
υ_{129}	$\delta C_{Me}NC_{Me}$ $_{+}\delta C_rNC_{Me}$	445	445	1.8	*ia*		-
υ_{130}	$\delta_{oop}CCC_{ring}$	381-435	365-417	*Ia*	0.4		398w
υ_{131}				2.7	*ia*		
υ_{132}	δ_{oop} ring def			*Ia*	8.1		
υ_{133}				9.6	*ia*		
υ_{134}				9.7	*ia*		
υ_{135}	δ_{ip} $C_1C_4C_7$	375	375	*Ia*	2.6		(330w)
υ_{136}	δ_{oop} C-N	332	318	*Ia*	1.4		(330w)
υ_{137}	τ torsion CH_3	298-188	298-188	16.7	*ia*	-	-
υ_{138}				*Ia*	3.5		266vvw
υ_{139}				1.4	ia		-
υ_{140}				3.4	0.06		
υ_{141}				0.01	11.9		247vvw
υ_{142}	γ C=N-C + γ N=C-C + τ CH_3			*Ia*	2.4		(222vvw)
υ_{143}				5.0	*ia*		
υ_{144}				*Ia*	5.1		
υ_{145}	δ_r twist + γ C-C-N	182-101	182-146	13.8	*ia*		(124w)
υ_{146}				3.8	*Ia*		
υ_{147}				*Ia*	5.0		
υ_{148}				*Ia*	8.5		
υ_{149}				6.9	*Ia*		
υ_{150}				7.6	0.3		
υ_{151}				1.0	1.3		

[a] Notations for fundamentals: s, symmetric; as, antisymmetric; ip, in-plane, oop, out-of-plane, ν, stretch, δ, bending; ρ, rocking; γ, wagging and τ, torsion,

[b] Calculated infrared intensities in km/mol from B3LYP/6-31+G(d).

[c] Calculated Raman activities in $Å^4$/amu. from B3LYP/6-31+G(d).

[d] Current study (vs; very strong, s; strong, m; medium, w; weak, vw; very weak, and sh; shoulder; r, ring; Me, methyl; ol, olefinic; ar, aromatic; a, active; ia, inactive; al, aliphatic; alchain, aliphatic chain.

11 fundamentals below 100 cm^{-1} were not included, it is beyond our Raman & spectrophotometer limits.

4. Conclusion

- IR and Raman spectral measurements of the synthesized Schiff-B were found consistent with the computed harmonic vibrational frequencies using DFT B3LYP/6-31+G(d).
- Aided by Normal coordinate analysis employing the atomic displacements in Cartesian coordinates, the proposed vibrational assignments herein are nearly comprehensive, confident, and trustworthy.
- A slightly distorted symmetric molecule with an inversion center is preferred by the estimated Raman activity, infrared intensities, and IR/Raman spectral observations.

- Spectroscopic analysis and calculated structural characteristics pronounce that both aromatic rings retain their aromaticity.

5. Conflicts of interest

"There are no conflicts to declare".

6. Formatting of funding sources

"There are no funding sources".

Acknowledgments

The authors gratefully thank the Egyptian Petroleum Research Institute and Al-Azhar University for their supports.

7. References

[1] E. Raczuk, B. Dmochowska, J. Samaszko-Fiertek, J. Madaj, Different Schiff Bases—Structure, Importance and Classification, Molecules 27(3) (2022) 787.

[2] Taha, R. H., Gaber, G. A., Mohamed, L. Z., & Ghanem, W. A. Corrosion inhibition of two schiff base complexes on the mild steel in 1M HCL solution. Egyptian Journal of Chemistry, *62* (2019) 381.

[3] Ghosh, P., Dey, S. K., Ara, M. H., Karim, K., & Islam, A. B. M. A review on synthesis and versatile applications of some selected Schiff bases with their transition metal complexes. Egyptian Journal of Chemistry, 62 (2019) 547.

[4] M. Smith, J. March, Aliphatic nucleophilic substitution, March's Advanced Organic Chemistry: Reactions, Mechanisms, and Structure 5 (2001) 389-674.

[5] D. Udhayakumari, V. Inbaraj, A review on Schiff Base fluorescent Chemosensors for cell imaging applications, Journal of Fluorescence 30(5) (2020) 1203-1223.

[6] Y. Wu, H. Cheng, Y. Chen, L. Chen, Z. Fang, L. Liang, Formation of a multiligand complex of bovine serum albumin with retinol, resveratrol, and (−)-epigallocatechin-3-gallate for the protection of bioactive components, Journal of agricultural and food chemistry 65(14) (2017) 3019-3030.

[7] H.F.G. Barbosa, M. Attjioui, A.P.G. Ferreira, E.R. Dockal, N.E. El Gueddari, B.M. Moerschbacher, É.T.G. Cavalheiro, Synthesis, characterization and biological activities of biopolymeric schiff bases prepared with chitosan and salicylaldehydes and their Pd (II) and Pt (II) complexes, Molecules 22(11) (2017) 1987.

[8] O. Berkesi, T. Körtvélyesi, C. Hetényi, T. Németh, I. Pálinkó, Hydrogen bonding interactions of benzylidene type Schiff bases studied by vibrational spectroscopic and computational methods, Physical Chemistry Chemical Physics 5(10) (2003) 2009-2014.

[9] J. Xu, Y. Liu, S.-h. Hsu, Hydrogels based on Schiff base linkages for biomedical applications, Molecules 24(16) (2019) 3005.

[10] N. Raman, S.F.S. Ali, D.J. Raja, Designing, synthesis and spectral characterization of Schiff base transition metal complexes: DNA cleavage and antimicrobial activity studies, Journal of the Serbian Chemical Society 73(11) (2008) 1063-1071.

[11] M.T. Kaczmarek, M. Zabiszak, M. Nowak, R. Jastrzab, Lanthanides: Schiff base complexes, applications in cancer diagnosis, therapy, and antibacterial activity, Coordination Chemistry Reviews 370 (2018) 42-54.

[12] A.M. Channa, A.N. Siyal, S.Q. Memon, S. Parveen, Design of experiment for treatment of arsenic-contaminated water using Schiff's base metal complex modified Amberlite XAD-2, Desalination and Water Treatment 57(8) (2016) 3664-3673.

[13] M. Lashanizadegan, H.A. Ashari, M. Sarkheil, M. Anafcheh, S. Jahangiry, New Cu (II), Co (II) and Ni (II) azo-Schiff base complexes: Synthesis, characterization, catalytic oxidation of alkenes and DFT study, Polyhedron 200 (2021) 115148.

[14] X.-L. Li, B. Xie, J.-S. Feng, C. Lai, X.-X. Bai, T. Li, D.-L. Zhang, W.-Y. Mou, L. Wen, Y.-T. Gu, 2-Pyridinecarboxaldehyde-based Schiff base as an effective corrosion inhibitor for mild steel in HCl medium: Experimental and computational studies, Journal of Molecular Liquids 345 (2022) 117032.

[15] M. Lashgari, M.-R. Arshadi, S. Miandari, The enhancing power of iodide on corrosion prevention of mild steel in the presence of a synthetic-soluble Schiff-base: electrochemical and surface analyses, Electrochimica Acta 55(20) (2010) 6058-6063.

[16] Hosny, Rania & Gaber, Ghalia & Mohamed, Lamiaa & Ghanem, Wafaa. Corrosion inhibition of two Schiff base complexes on the mild steel in 1M HCl solution. Egyptian Journal of Chemistry. 10.21608/ejchem. (2019).1722.

[17] E.M. Zayed, G. Mohamed, Synthesis, spectroscopic, DFT and docking studies, molecular

structure of new Schiff base metal complexes, Egyptian Journal of Chemistry 65(1) (2022) 1-2.
[18] M. Meenukutty, A.P. Mohan, V. Vidya, V.V. Kumar, Synthesis, characterization, DFT analysis and docking studies OFA novel schiff base using 5-bromo salicylaldehyde and β-alanine, Heliyon (2022) e09600.
[19] G. Kotan, S. Manap, H. Yüksek, Synthesis, Characterization, Antioxidant and DFT Studies of Some Novel Schiff Base Compounds, Journal of Computational Biophysics and Chemistry 21(1) (2022) 47-63.
[20] J. Anacona, J. Santaella, R.K.R. Al-Shemary, J. Amenta, A. Otero, C. Ramos, F. Celis, Ceftriaxone-based Schiff base transition metal (II) complexes. Synthesis, characterization, bacterial toxicity, and DFT calculations. Enhanced antibacterial activity of a novel Zn (II) complex against S. aureus and E. coli, Journal of Inorganic Biochemistry 223 (2021) 111519.
[21] C. Arunagiri, A. Subashini, M. Saranya, P.T. Muthiah, K. Thanigaimani, I.A. Razak, Synthesis, crystal structure and theoretical studies of a Schiff base 2-[4-hydroxy benzylidene]-amino naphthalene, Spectrochimica Acta Part A: Molecular and Biomolecular Spectroscopy 135 (2015) 307-316.
[22] S.O. Smith, A.B. Myers, R.A. Mathies, J.A. Pardoen, C. Winkel, E. van Den Berg, J. Lugtenburg, Vibrational analysis of the all-trans retinal protonated Schiff base, Biophysical journal 47(5) (1985) 653-664.
[23] A. Filarowski, A. Koll, L. Sobczyk, Vibrational spectra of o-hydroxyphenyl Schiff bases and related compounds, Current Organic Chemistry 13(3) (2009) 287-298.
[24] S.I. Touw, H.J. de Groot, F. Buda, Ab initio modeling of the spatial, electronic, and vibrational structure of Schiff base models for visual photoreceptors, The Journal of Physical Chemistry B 108(35) (2004) 13560-13572.
[25] J. Antunes, L. Silva, R. Bento, A. Teixeira, P. Freire, J. Faria, R. Ramos, C. Silva, J. Lima Jr, Vibrational spectra and DFT calculations of the vibrational modes of Schiff base C18H17N3O2, Journal of Molecular Structure 1013 (2012) 126-133.
[26] L. Guo, T. Ji, C. Liu, Y. Li, Y. Huang, Y. Mo, J. Zhao, The Raman vibrational characteristics and assignments of three Schiff bases, Guang pu xue yu Guang pu fen xi= Guang pu 21(3) (2001) 317-319.
[27] S. Masuda, H. Torii, M. Tasumi, Vibrational Analysis of a Schiff Base Based on ab Initio Molecular Orbital Calculations: Effect of Electron Correlation on the CN Stretching Force Constant and the Origin of the Shift of the CN Stretching Frequency upon Protonation and Hydrogen-Bond Formation, The Journal of Physical Chemistry 100(38) (1996) 15328-15334.
[28] A.D. Becke, Density-functional exchange-energy approximation with correct asymptotic behavior, Physical Review A 38(6) (1988) 3098-3100.
[29] Abdu, A. N., & Migahed, M. A. Experimental and theoretical insights into synthesized Gemini corrosion inhibitor for X65-steel in 1M HCl. Egyptian Journal of Chemistry (2022).
[30] Migahed, M. A., Nasser, A., Elfeky, H., & El-Rabiei, M. M. The synthesis and characterization of benzotriazole-based cationic surfactants and the evaluation of their corrosion inhibition efficiency on copper in seawater. RSC advances, 9(46) (2019) 27082.
[31] Jebin, R. P., T. Suthan, N. P. Rajesh, G. Vinitha, and U. Madhusoodhanan. "Growth and characterization of organic material 4-dimethylaminobenzaldehyde single crystal." Spectrochimica Acta Part A: Molecular and Biomolecular Spectroscopy 135 (2015): 959-964
[32] Campetella, M., Cappelluti, F., Fasolato, C., Conte, D., Palumbo, O., Paolone, A., ... & Gontrani, L. Physical-chemical studies on putrescine (butane-1, 4-diamine) and its solutions: Experimental and computational investigations. Journal of Molecular Liquids, 322, (2021), 114568.
[33] W. Hehre, L. Radom, P. v R. Schleyer, and JA Pople. Ab initio molecular orbital theory, 1986.
[34] A.D. Becke, Density-functional exchange-energy approximation with correct asymptotic behavior, Physical review A 38(6) (1988) 3098.
[35] C. Lee, W. Yang, R.G. Parr, Development of the Colle-Salvetti correlation-energy formula into a functional of the electron density, Physical review B 37(2) (1988) 785.
[36] A. Ambrosetti, D. Alfè, R.A. DiStasio Jr, A. Tkatchenko, Hard numbers for large molecules: Toward exact energetics for supramolecular systems, The Journal of Physical Chemistry Letters 5(5) (2014) 849-855.
[37] S. Grimme, A simplified Tamm-Dancoff density functional approach for the electronic excitation

spectra of very large molecules, The Journal of chemical physics 138(24) (2013) 244104.
[38] R.K. Roy, S. Saha, Studies of regioselectivity of large molecular systems using DFT based reactivity descriptors, Annual Reports Section" C"(Physical Chemistry) 106 (2010) 118-162.
[39] C. Møller, M.S. Plesset, Note on an approximation treatment for many-electron systems, Physical review 46(7) (1934) 618.
[40] K. Kristensen, I.-M. Høyvik, B. Jansik, P. Jørgensen, T. Kjærgaard, S. Reine, J. Jakowski, MP2 energy and density for large molecular systems with internal error control using the Divide-Expand-Consolidate scheme, Physical Chemistry Chemical Physics 14(45) (2012) 15706-15714.
[41] Y. Nakao, K. Hirao, A local second-order Møller–Plesset method with localized orbitals: A parallelized efficient electron correlation method, The Journal of chemical physics 120(14) (2004) 6375-6380.
[42] P. Maslen, M. Head-Gordon, Non-iterative local second order Møller–Plesset theory, Chemical physics letters 283(1-2) (1998) 102-108.
[43] S. Saebø, P. Pulay, A low-scaling method for second order Møller–Plesset calculations, The Journal of Chemical Physics 115(9) (2001) 3975-3983.
[44] L. Ravichandran, S. Banik, Investigation of the Failure of the MP2 Method to Describe the Out-of-Plane Bending Motions of Carbon–Carbon Double-Bonded Molecules: The Role of Atomic Orbitals, The Journal of Physical Chemistry A 125(42) (2021) 9298-9317.
[45] E. Soydas, U. Bozkaya, Assessment of orbital-optimized MP2. 5 for thermochemistry and kinetics: dramatic failures of standard perturbation theory approaches for aromatic bond dissociation energies and barrier heights of radical reactions, Journal of Chemical Theory and Computation 11(4) (2015) 1564-1573.
[46] M. Frisch, F. Clemente, Gaussian 09, revision a. 01, mj frisch, gw trucks, hb schlegel, ge scuseria, ma robb, jr cheeseman, g, Scalmani, V. Barone, B. Mennucci, GA Petersson, H. Nakatsuji, M. Caricato, X. Li, HP Hratchian, AF Izmaylov, J. Bloino, G. Zhe (2009) 20-44.
[47] P. Pulay, Ab initio calculation of force constants and equilibrium geometries in polyatomic molecules: I. Theory, Molecular Physics 17(2) (1969) 197-204.
[48] N. Colthup, Introduction to infrared and Raman spectroscopy, Elsevier2012.
[49] L. Bellamy, The infra-red spectra of complex molecules, Springer Science & Business Media2013.
[50] R.K. Heenan, L.S. Bartell, Electron diffraction studies of supersonic jets. IV. Conformational cooling of n-butane, The Journal of Chemical Physics 78(3) (1983) 1270-1274.
[51] J. Durig, A. Wang, W. Beshir, T. Little, Barrier to asymmetric internal rotation, conformational stability, vibrational spectra and assignments, and Ab Initio calculations of n-butane-d0, d5 and d10, Journal of Raman spectroscopy 22(11) (1991) 683-704.
[52] R. Bonham, L. Bartell, The Molecular Structure and Rotational Isomerization of n-Butane1, 2, Journal of the American Chemical Society 81(14) (1959) 3491-3496.
[53] L. Sundararaman, H. Ramu, R. Kandaswamy, H. Stoeckli-Evans, (E)-4-[(4-Methoxyphenyl) iminomethyl]-N, N-dimethylaniline, Acta Crystallographica Section E: Structure Reports Online 65(3) (2009) o477-o477.
[54] J.a.K. Jawad, T.A. Mohamed, U.A. Soliman, L.D. Wilson, A.M. Abuelela, Raman and infrared spectra, crystal structure and DFT calculations of novel N-benzyl-4-(3-benzylcarbamoyl-propyldisulfanyl)-butyramide:[C6H5CH2NHC (O)(CH2) 4S] 2, Research on Chemical Intermediates 41(7) (2015) 4761-4784.
[55] K. Kuchitsu, Electron diffraction investigation on the molecular structure of n-butane, Bulletin of the Chemical Society of Japan 32(7) (1959) 748-769.
[56] W. Bradford, S. Fitzwater, L.S. Bartell, Molecular structure of n-butane: calculation of vibrational shrinkages and an electron diffraction re-investigation, Journal of Molecular Structure 38 (1977) 185-194.
[57] J. Rumble, CRC handbook of chemistry and physics. 102nd edition 2021–2022, CRC Press, Boca Raton, London, New York, 2021.
[58] A. Habenschuss, A. Narten, X-ray diffraction study of liquid n-butane at 140 and 267 K, The Journal of chemical physics 91(7) (1989) 4299-4306.
[59] J. Schachtschneider, Vibrational Analysis of Polyatomic Molecules, VI: FORTRAN IV Programs for Solving the Vibrational Secular Equation and for the Least-Squares Refinement of Force Constants, Shell Development Company1965.

[60] G.A. Guirgis, Y.D. Hsu, A.C. Vlaservich, H.D. Stidham, J.R. Durig, Vibrational spectrum, ab initio calculations, assignments of fundamentals, barriers to internal rotation and stabilities of conformers of 1, 2-dichloropropane, Journal of molecular structure 378(2) (1996) 83-102.
[61] E.B. Wilson, JC Decius, and PC Cross, Molecular Vibrations, The Theory of Infrared and Raman Vibrational Spectra. McGraw-Hill, New York (1955).
[62] A.M. Abuelela, T.A. Mohamed, O.V. Prezhdo, DFT simulation and vibrational analysis of the IR and Raman spectra of a CdSe quantum dot capped by methylamine and trimethylphosphine oxide ligands, The Journal of Physical Chemistry C 116(27) (2012) 14674-14681.
[63] R. Dennington, T. Keith, J.G. Millam, Version 5, Semichem Inc.: Shawnee Mission, KS, USA (2009).
[64] P. Larkin, Infrared and Raman spectroscopy: principles and spectral interpretation, Elsevier2017.
[65] A. Burrill, P. Johnson, Torsional analyses of trans-2-butene and propene cations: A comparative investigation of two prototypical ions with different degrees of symmetry, The Journal of chemical physics 115(1) (2001) 133-138.
[66] S. Dash, R.K. Singh, P. Alapati, A. Verma, A comparative laser Raman study on TB4A, TB7A and TB10A, Liquid crystals 25(4) (1998) 459-465.
[67] N.C. Handy, P.E. Maslen, R.D. Amos, J.S. Andrews, C.W. Murray, G.J. Laming, The harmonic frequencies of benzene, Chemical physics letters 197(4-5) (1992) 506-515.
[68] U.A. Soliman, A.M. Hassan, T.A. Mohamed, Conformational stability, vibrational assignmenents, barriers to internal rotations and ab initio calculations of 2-aminophenol (d0 and d3), Spectrochimica Acta Part A: Molecular and Biomolecular Spectroscopy 68(3) (2007) 688-700.
[69] T.A. Mohamed, G.A. Guirgis, Y.E. Nashed, J.R. Durig, Spectra and Structure of Silicon-Containing Compounds. XXV. Raman and Infrared Spectra, r 0 Structural Parameters, Vibrational Assignment, and Ab Initio Calculations of Ethyl Chlorosilane-Si-d2, Structural Chemistry 10(5) (1999) 333-348.
[70] A.M. Abuelela, U.A. Soliman, G.A. El-hagali, W.M. Zoghaib, T.A. Mohamed, Synthetic routes and vibrational analysis of 5-(4-Chlorophenyl)-3H-pyrazol-3-one molecule: Raman, Infrared and DFT calculations, Journal of Molecular Structure 1245 (2021) 131036.